Phase decomposition and its applications

Satinder Chopra[1*], Ritesh Kumar Sharma[1], John Castagna[2], Oleg Portniaguine[3], Gabriel Gil[3] and Kenneth Bredesen[4].

Abstract

We discuss the recently introduced phase decomposition analysis, which entails amplitude variation with time for a specific seismic phase. Assuming a zero-phase wavelet embedded in the seismic data, while flat spots or unresolved water contacts may be seen on the zero-phase component, thin-bed and impedance changes will show up on phase components that are 90° out of phase with the wavelet. Similar bright spots caused by thin hydrocarbon reservoirs are associated with low impedance and show up on the phase component that is -90° out of phase with the embedded wavelet. In all cases the interpretation of bright spots is found to be convenient, and easier with the use of -90° seismic phase component. In this paper, application of phase decomposition to a few instances are first demonstrated through synthetic data examples, followed by a couple of real seismic data case studies. In particular, the case study from a gas storage reservoir in Denmark exhibits how phase decomposition can aid interpretation efforts. Some of the typical issues that seismic interpreters might come across, including the one where the input seismic data might have a phase different from zero phase are elaborated in the 'Discussion' section.

Introduction

Phase decomposition is a novel technique that decomposes a composite seismic signal into different phase components, which can improve reservoir characterization. The technique is particularly useful in those areas where thin-bed interference causes the phase of the input seismic response to differ from the phase of the embedded wavelet in the data. For a zero-phase wavelet in the data and thin low-impedance layers below tuning thickness, the waveform phase response generated after carrying out phase decomposition is found to be -90°, which stands out anomalously. On the contrary, a corresponding high-impedance thin layer exhibits a similar +90° phase waveform response. By generating a synthetic response with use of well data and a zero-phase wavelet, such observations for thin reservoir layers can be understood with confidence and correlated with real seismic data. Phase decomposition can help immensely in direct interpretation of seismic data in terms of reservoir and non-reservoir zones, among other applications.

Another important aspect is that the seismic waveform is amplitude, phase, and frequency dependent. Consequently, for thin layers below tuning, the frequency content of the associated seismic response must be monitored for targets with variable thicknesses. Phase decomposition does not use well data for the generation of phase components, but the synthetic traces generated from well data can be used to establish the relationships between amplitude/phase/frequency for a given problem. In this context, application of spectral decomposition to a synthetic trace would produce a frequency gather and provide the required frequency dependent behaviour. Likewise, the application of phase decomposition to the generated synthetic gather will provide a set of phase component gathers. Thus, between the spectral and phase decomposition applications, the desired amplitude/phase/frequency information can be found.

We begin this article with a brief description of some of the spectral decomposition techniques available in different commercial software packages, and then showcase their application to a seismic dataset under study. We take the discussion forward from there to the description of phase decomposition and its applications. Finally, we draw some convincing conclusions.

Spectral decomposition

Spectral decomposition is an effective way of analysing the seismic response of stratigraphic geologic features. It is carried out by transforming the seismic data from the time domain into the frequency domain. This can be done simply by using the short time window discrete Fourier transform (STFT; Partyka et al.,1999), but there are other methods that can be used for the purpose, namely the continuous wavelet transform (CWT; Chakraborty and Okaya, 1995; Sinha et al., 2005), S-transform (Stockwell et al., 1996), matching pursuit (Mallat and Zhang, 1993), constrained least-squares spectral analysis (CLSSA; Puryear et al., 2012), and the optimal Gaussian spectral analysis (OGSA; Lindner et al.,2014). Some of these methods have been used extensively in reservoir characterization exercises, and the literature is replete with different case studies. Using any of the above spectral decomposition methods, the input seismic data volume is decomposed into amplitude and phase volumes at discrete frequencies within the

[1] SamiGeo | [2] The University of Houston | [3] Lumina Technologies Inc. | [4] Geological Survey of Denmark and Greenland (GEUS)
[*] Corresponding author, E-mail: Satinder.Chopra@samigeo.com
DOI: xxx

bandwidth of the data, which can then be displayed and interpreted. Alternatively, the output data can be sorted into time-frequency displays, also called gathers, for amplitude and phase.

In this article we begin with a comparison of the frequency gathers for amplitude and phase generated with the application of the following methods.

- STFT: The discrete Fourier transform uses a time window for its computation, and this choice has a bearing on the resolution of the output data.
- CWT: The continuous wavelet transform depends on the choice of the mother wavelet, and usually yields higher spectral resolution but reduced temporal resolution at low frequencies.
- CLSSA: Uses an inversion-based algorithm for computing the spectral decomposition of seismic data and is performed by the inversion of a basis of truncated sinusoidal kernels in a short time window. The method results in a time-frequency analysis with excellent time and frequency resolution and with a time-frequency product superior to the STFT and the CWT.
- OGSA: This process uses a series of frequency domain Gaussian functions to decompose the spectrum of the data, which is carried out in the frequency domain. The result is the superposition of frequency domain Gaussian functions that are seen to better correlate or match the spectrum of the seismic data.

In Figure 1 we show the spectral amplitude gathers for a particular seismic trace shown to the left. We see that these amplitude gathers generated with the application of some of the methods mentioned above are comparable, though differing in temporal and frequency resolution. However, we also notice that the equivalent phase gathers generated by the same set of methods and displays in Figure 2 appear to be complicated in terms of their interpretative value.

Phase decomposition

Castagna et al. (2016) introduced an alternative approach for understanding the phase of the seismic trace by distributing the amplitude and phase spectra such that the amplitude can be

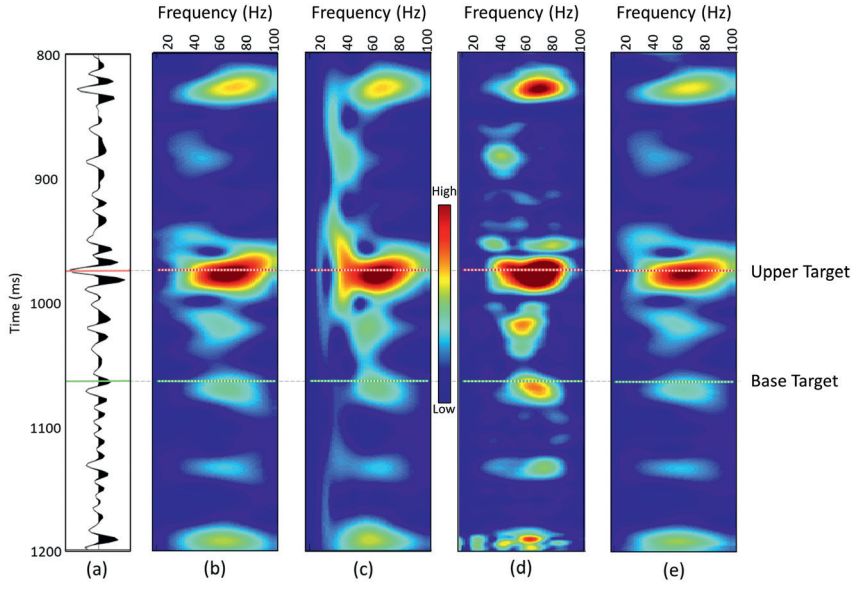

Figure 1 Spectral decomposition on a seismic trace in (a) with the generated amplitude frequency gathers using the (b) STFT (40 ms window), (c) CWT, (d) CLSSA (40 ms window), and (e) OGSA methods. The two horizontal dotted lines in red and green are the levels of the two markers shown for reference.

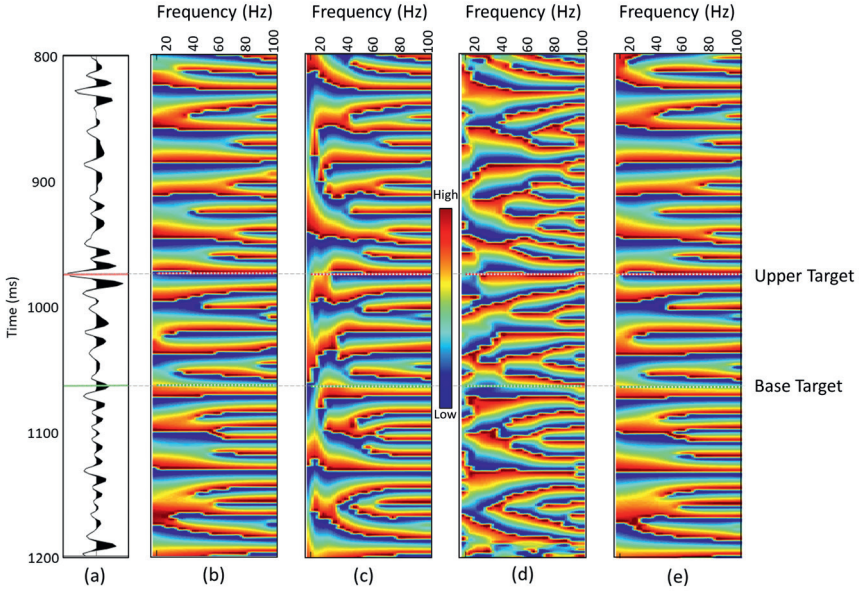

Figure 2 Spectral decomposition on a seismic trace in (a) with the generated phase frequency gathers using the (b) STFT (40 ms window), (c) CWT, (d) CLSSA (40 ms window), and (e) OGSA methods. The two horizontal dotted lines in red and green are the levels of the two markers shown for reference.

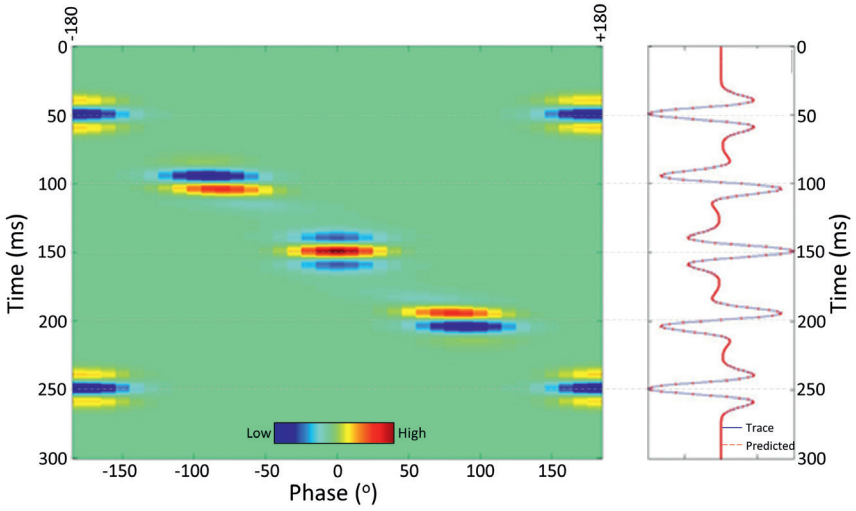

Figure 3 Illustration of seismic phase decomposition. A synthetic seismic trace (solid blue) is shown to the right and the generated time-phase panel or phase gather for it is shown to the left. When the time-phase panel is summed over phase, the original trace is reconstructed and is shown overlaid as dashed red on the solid blue trace to the right.

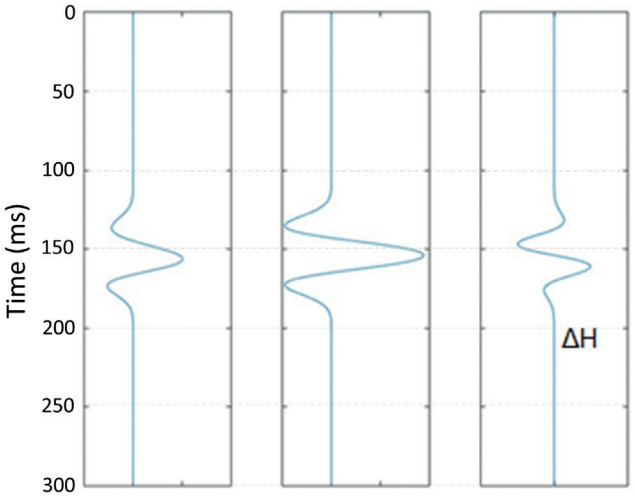

Figure 4 Synthetic waveforms for a seismically thin layer using a zero-phase wavelet resulting in a 'dim spot' when gas is added. Both brine and gas-filled cases have intermediate impedance between the overlying and underlying impedances, yielding a zero-phase waveform for both cases. Notice the hydrocarbon effect, ΔH, has a -90° phase rotation with respect to the nearly zero-phase wavelet.

expressed as a function of phase as well as frequency. In general, as stated above, the application of spectral decomposition on a seismic trace produces a time-frequency analysis, which when integrated over the data frequency range will recover the original trace. In this analysis it is possible to introduce phase as a third dimension such that a time-phase analysis, or a phase gather, can be generated, which essentially represents the amplitude as a function of time for individual phase components of the seismic trace. When integrated over the complete phase range, the original seismic trace can be reconstructed.

For gaining an insight into this process, a synthetic seismic trace generated with the use of a few Ricker wavelets is shown in solid blue to the right in Figure 3. To the left is the phase gather generated for the blue synthetic seismic trace, which exhibits a good correlation with the phase information indicated on the original seismic trace. On summing this time phase panel over phase, the original seismic trace can be reconstructed and is shown as a dashed red trace overlaid on the solid blue original trace. An interesting observation that can be made here is that any phase component of the seismic trace as seen on the phase panel can be extracted and reconstructed. A significant implication of this observation is that phase decomposition can be used as a powerful tool that may be put to use for accentuating or suppressing seismic events with specific spectral characteristics. This process is referred to as ***phase filtering***.

As mentioned in the introduction, a unique difference in response between thin hydrocarbon-bearing reservoirs exhibiting low impedance and the same reservoir rock with 100% water saturation and higher impedance is found to occur on the phase component that is out of phase with the embedded zero-phase seismic wavelet. Before going into the details of the phase decomposition method, we wish to demonstrate this. Figure 4 shows a zero-phase response representing a brine-filled thin layer with impedance intermediate between overlying and underlying half-spaces (middle) as well as the waveform associated with a similar layer bearing gas, also with intermediate impedance (left panel). For seismically thin layers, the gas response minus the brine response, called the ***hydrocarbon effect*** (right panel) is always -90° phase rotated with respect to the zero-phase wavelet.

To get a feel for the benefits of phase decomposition, we can look at the synthetic example of an intermediate impedance thin layer (with layer time thickness equal to quarter of the dominant wavelet period) as shown in Figure 5a. The layer itself has a channel with reduced impedance relative to the inter-channel facies. The modelled synthetic response is shown in Figure 5b and the -90° phase component response is shown in Figure 5c. The wavelet used for generating the seismic response is a zero-phase Ricker wavelet, and the modelled response is displayed with SEG polarity, i.e., a positive reflection coefficient is represented as a peak. This polarity convention is used for all displays shown in this article.

The slight changes in amplitude caused by the channel change the reflection coefficients slightly, but the lateral variation in the amplitude caused by the channel is small enough and may not be recognized on conventional seismic data. This implies that any amplitude or phase anomaly that we may expect due to the channel will be weak and may not be detected on the seismic traces.

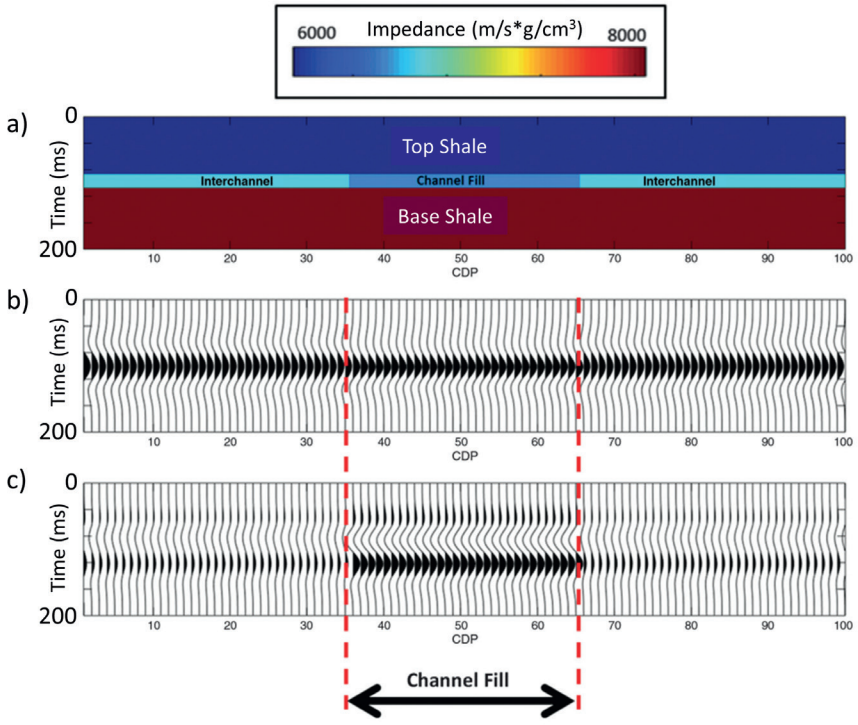

Figure 5 (a) A hypothetical geological model showing a change in impedance in the thin layer containing a channel. (b) Modeled synthetic amplitude response does not show the amplitude anomaly corresponding to the thin impedance layer, and (c) the computed –90° phase component exhibits a strong amplitude anomaly for the thin impedance channel. (Castagna et al., 2016).

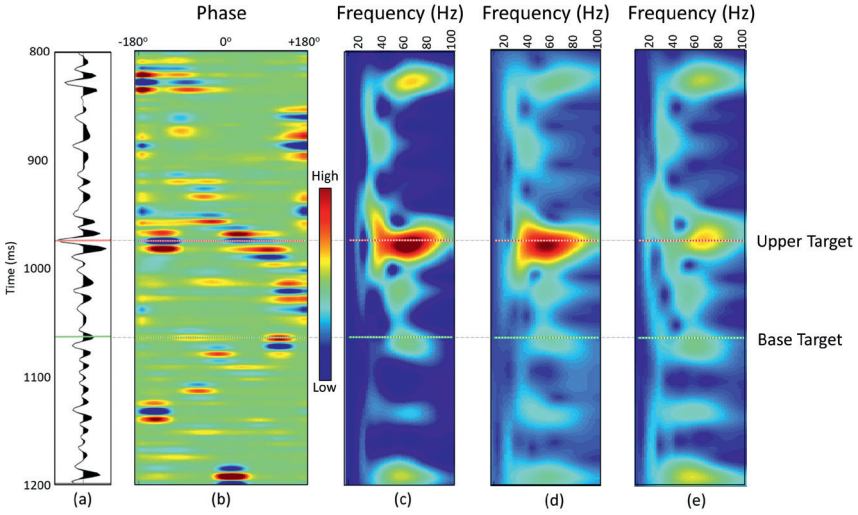

Figure 6 (a) A trace from a 3D seismic volume from Denmark. (b) Phase gather generated for the seismic trace in (a). (c) Frequency gather generated for the seismic trace in (a) using the CWT method, with the computed odd and even component gathers shown in (d) and (e). The two horizontal dotted lines in red and green are the levels of the two markers shown for reference.

The -90° phase component is nicely shown in Figure 5c as a prominent anomaly in what is almost invisible in Figure 5b.. Thus, for thin layers the change in waveform corresponding to an anomalously low impedance is expected to show up on the -90° phase component, and conversely, the change in waveform caused by an anomalously high impedance will occur on the +90° phase component. Intermediate impedance changes as well as lateral impedance changes are visible on the ±90° phase components. Both these phase components (-90° and +90°) could be added to produce an output that may be referred to as the *odd component*; similarly, the 0° and 180° phase components could be summed to produce what may be referred to as the *even component*. Such observations suggest that phase decomposition could serve as a tool for direct interpretation of data in terms of impedance variations.

Likewise, phase decomposition can be used as a reconnaissance tool when hydrocarbon anomalies associated with a range of thicknesses are expected to be seen on seismic data. The resolved reflections on the different phase components may not show any difference from the zero-phase input seismic data. But the bright spots associated with thin low-impedance gas sands may exhibit a strong anomaly on the -90° phase component.

Real data application

The seismic data used for the first phase decomposition application is a 3D seismic volume from Denmark shot over a natural gas storage structure. Natural gas has been injected and stored in this structure since 1989, where the reservoir occurs within a domal subsurface structure and is covered by a tight caprock. The 'Gassum target interval' bounded by Upper Target and Base Target markers (Figure 7a), approximately 140 m-thick consists of interbedded sandstones and mudstones and is the reservoir where natural gas is stored by displacing formation water. The upper

40 m are divided into five gas storage zones segregated by thin shale beds, which operate as two separated units, namely Zones 1-3 operate as one integrated unit and is located approximately 22 ms below, and Zone 5 which is located close to 38 ms below the Upper Target marker.

Overlying the Upper Target marker is the 300 m thick Lower Jurassic sandstone Formation (not shown), which consists of marine mudstones and shales, and is the regional caprock. Below the Base Target marker are the impermeable mudstones of older formations (not shown), at approximately 2800 m below the surface.

In Figure 6 we show the same seismic trace shown in Figure 1 together with the frequency gather generated using the CWT method and the corresponding odd and even component gathers. The equivalent phase gather is shown to the left of the seismic trace. We notice a prominent anomaly seen on the frequency gather, the phase gather, and which is also prominently seen on the odd frequency gather, but not on the even component.

Finally, in Figure 7a we show a segment of an inline from the seismic data volume. A prominent amplitude anomaly is seen in the middle of the section and its extent is indicated with the yellow block arrows. Figures 7b and c show the equivalent even and odd sections generated after phase decomposition was carried out on the input seismic data. Notice how no significant anomaly is seen on the even component but stands out clearly on the odd component.

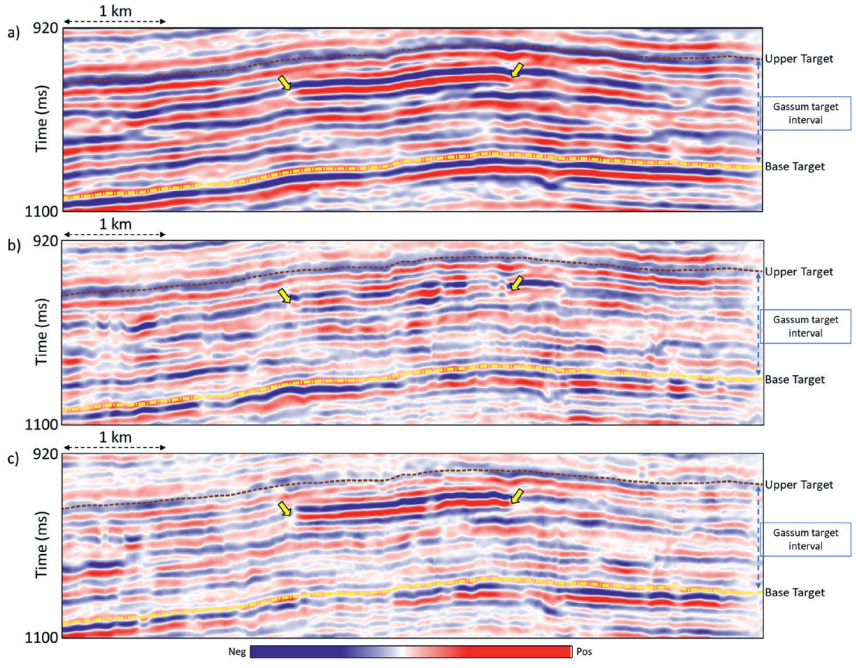

Figure 7 (a) An inline section from the PSTM stacked volume showing a shallow high-amplitude gas anomaly indicated with a yellow block arrow. (b) Equivalent inline section from the even phase (combination of 0° and 180° event phases) component volume. (c) Equivalent inline section from the odd phase (combination of -90° and +90° event phases) component volume.

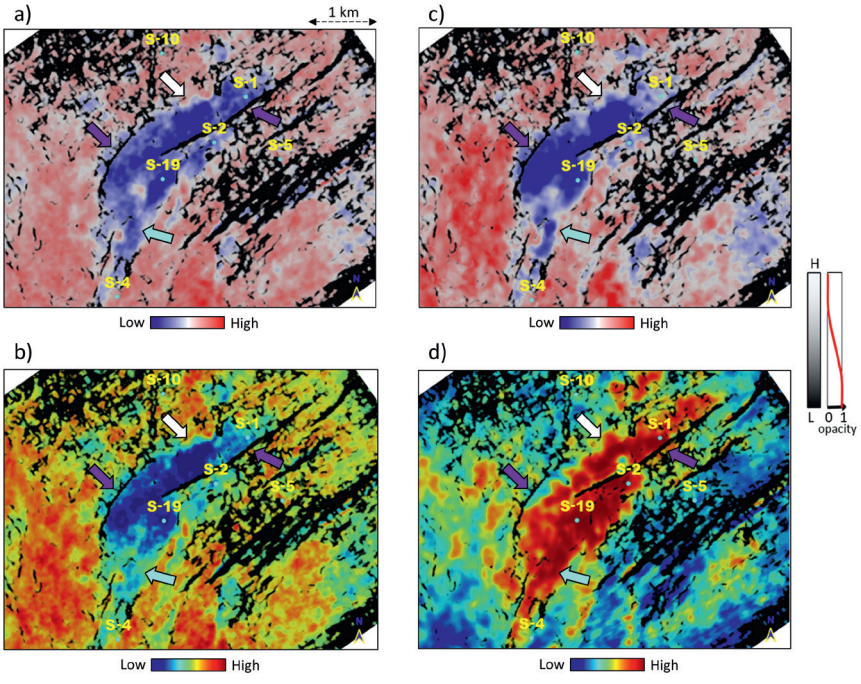

Figure 8 Stratal slices at the level of gas zone 3 from (a) input seismic data, (b) relative acoustic impedance data derived by integration of reflection coefficients derived from input seismic data through spectral inversion, (c) odd phase component stacked data, and the (d) gas sandstone probability volumes. The gas probability volume was generated using probabilistic impedance inversion (Bredesen, 2021). On each display multispectral coherence has been overlaid in black using transparency. The odd phase component display appears to be less patchy and laterally more continuous than the seismic, relative acoustic impedance, or the gas probability displays.

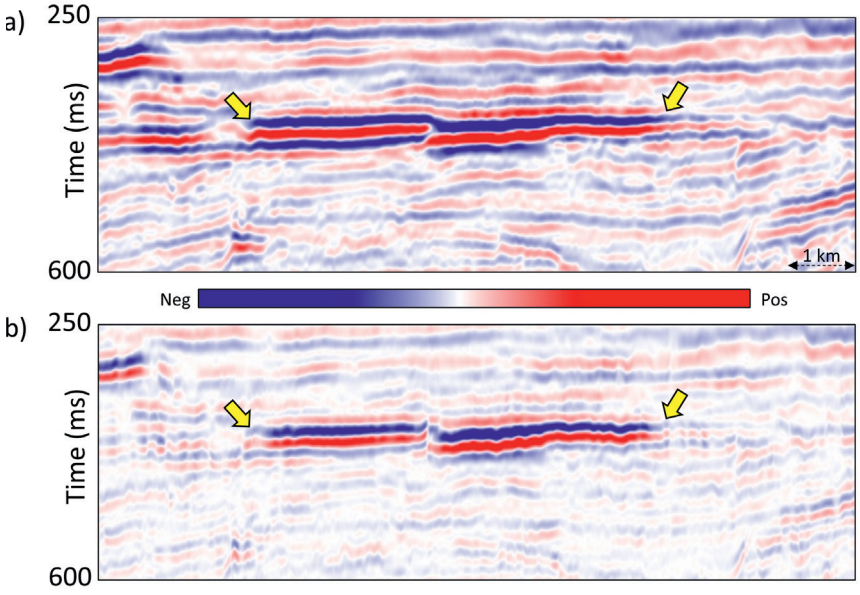

Figure 9 (a) An inline section from far-angle stack showing a shallow high-amplitude anomaly indicated with a pair of yellow block arrows. (b) Equivalent inline section from the odd phase (combination of -90° and +90° phase components) component volume. Notice the clarity with which the anomaly stands out.

In Figure 8a, the seismic stratal slice shows the gas anomaly in blue with the wells ST-01, 02, 04 and 19 touching it, implying they are associated with storage or retrieval of gas in the reservoir. Multispectral coherence (Chopra and Marfurt, 2018) has been overlaid in black, using transparency. The equivalent display in Figure 8b is from the relative acoustic impedance volume generated by integration of reflection coefficients extracted from the input seismic data using spectral inversion (Portniaguine and Castagna, 2004, 2005). Interestingly, on this display, at the location of the light blue arrow the dark blue colour fades, suggesting that the reflection coefficients there are very small. On the equivalent display from the odd phase (a combination of -90° and +90° phase components) component volume shown in Figure 8c, the blue anomaly is seen as more compact, exhibiting better variation as compared with the other two displays. Besides, the faults marked with purple block arrows appear to be acting as fluid barriers, with the relative impedance and odd phase component following them closely. Another encouraging observation is about the extent of gas migration towards southwest in the direction of well S-4, which appears to be more convincing on Figure 8c than 8a. The equivalent display shown in Figure 8d is from the gas probability volume was generated using probabilistic impedance inversion using stacked input seismic data (Bredesen, 2021). We notice that the anomaly corresponding to gas probability is spread out and does not exhibit a more constrained fluid distribution as the seismic odd phase component (Figure 8c). It may be appropriately mentioned here that in a reservoir management context, small deviations in the spatial extent of a hydrocarbon anomaly as seen on different map displays could be valuable information in order to improve the understanding of fluid movement within the reservoir. Thus, what we surmise from these observations is that the odd phase component can provide detailed information, which may be more accurate than when seen on the input seismic amplitudes.

Finally, Figure 9 exhibits another comparison of a seismic amplitude anomaly on far-angle stack (Figure 9a), and its equivalent anomaly seen on the odd phase (combination of -90° and +90° event phases) component display (Figure 9b). Again, the seismic amplitude anomaly is seen very clearly on the odd component display in the absence of any other seismic reflection event close by. The seismic data shown here are from the Taranaki Basin, which lies offshore on the western side of the North Island of New Zealand and was processed in 2015 to zero phase.

Discussion

In many regions around the world the production is expected from thin sandstone or carbonate reservoirs. Because the seismic waves are bandlimited with low-frequency content, a thin reservoir implies that the thickness of the reservoir is at or less than a quarter wavelength of the seismic waves (following Widess's (1973) criterion). Thus, if the average spectrum of a seismic wavelet is centered around 30Hz, which is usually the case, reservoirs having a thickness of less than 25 m may not have their top and base reflectors resolved. This may suffice for structural objectives, but stratigraphic targets are usually set to look for reservoirs 10 m or less in thickness. In such thin reservoirs the reflection response would comprise interference of reflections from the top and the base of the thin layers. Exercises aimed at characterizing thin reservoirs frequently neglect such interference effects, resulting in inaccurate reservoir characterization.

The phase decomposition discussed above finds useful applications subject to some caveats in that the seismic data being considered have a zero-phase embedded wavelet, the thicknesses of the zones of interest are at or below tuning at the CWT frequency used and the seismic response has an absence of interference from adjoining reflectors. The application of phase decomposition to data that may not have one or more of the above conditions satisfied may not yield optimum results.

The first question that pops up then is, what happens when the embedded wavelet in the seismic data is different from zero-phase? If the input seismic data are not zero-phase then attempts could be made to get the data reprocessed to zero phase for a meaningful application of phase decomposition. Not only that,

zero-phase data will help with more accurate interpretation. If that is not possible for some reason, i.e., if the seismic wavelet is not zero phase, the phase component where specific responses are expected, should be modified accordingly. For example, if a -90° signal is expected with a zero-phase wavelet, that response would be found on the -60° component if the wavelet phase were 30°.

If the layer of interest is above seismic tuning, low-pass filtering (for example by stacking low CWT frequencies) can be used to lower the frequency content and push the layer of interest below tuning. This is called ***seismic thinning***, and its applications for distinguishing target anomalies have been discussed by Meza et al. (2016) and Barbato et al. (2017).

Attempts should be made to alleviate such problems and could include wavelet shaping of the embedded wavelet if it is not zero phase, using CWT spectral decomposition with a Ricker wavelet at higher frequency (but not high enough to go above tuning), and finally the phase decomposition analysis could be carried out on the required phase as read off from the phase gather, or what may be referred to as phase filtering. Though not discussed here, some of these issues will be discussed in future articles.

Conclusions

Phase decomposition can be used as a tool for direct interpretation of data in terms of impedance variations as well as a reconnaissance tool. For doing these interpretations, not only the phase gathers but the individual phase components can also be generated, the ones at 0°, 180°, -90° and +90° appearing to be most useful. The first two phase components can be combined into an even component volume, and the latter two into an odd component volume. Thin-bed seismic anomalies associated with hydrocarbons can be conveniently analysed by interpreting these two data volumes.

References

Barbato, U., Portniaguine, O. Winkelman, B. and Castagna, J.P. [2017]. Phase decomposition as a DHI in bright spot regimes: A Gulf of Mexico case study. 87th Annual International Meeting, SEG, Expanded Abstracts, 3976-3980, doi.org/10.1190/segam2017-17737608.1.

Bredesen, K. [2021]. Assessing rock physics and seismic characteristics of the Gassum Formation in the Stenlille aquifer gas storage – A reservoir analog for the Havnsø CO_2 storage prospect, Denmark, accepted for publication in the *International Journal of Greenhouse Gas Control*.

Castagna, J., Sun, S. and Siegfried, R. [2003]. Instantaneous spectral analysis: Detection of low-frequency shadows associated with hydrocarbons. *The Leading Edge*, **22**(2), 120-127, doi.org/10/1190/1.1559038.

Castagna, J.P., Oyem, A., Portniaguine, O. and Aikulola, U. [2016]. Phase decomposition. *Interpretation*, **4**(3), SN1–SN10, dx.doi.org/10.1190/INT-2015-0150.1.

Chakraborty, A., and Okaya, D. [1995. Frequency-time decomposition of seismic data using wavelet-based methods. *Geophysics*, **60**(6), 1906–1916, doi.org/10.1190/1.3627561.

Chopra, S., and Marfurt, K.J. [2018]. Multispectral, multiazimuth and multioffset coherence attribute applications. *Interpretation*, **7**(2), SC21-SC32. doi.org/10.1190/INT-2018-0090.1.

Lindner, R.R., Vera-Ciro, C., Murray, C.E., Stanimirovic, S., Babler, B., Heiles, C., Hennebelle, P., Goss, W.M. and Dickey, J. [2015]. Autonomous Gaussian Decomposition. *The Astronomical Journal*, **148**(4) 1-14, doi:10.1.1088/0004-6256/149/4/138.

Mallat, S. and Z. Zhang [1993]. Matching pursuits with time-frequency dictionaries. *IEEE Transactions on Signal Processing,* **41**(12),3397–3415, doi:10.1109/78.258082.

Meza, R., Haughey, G., Castagna, J.P., Barbato, U. and Portniaguine O.[2016]. Phase decomposition as a hydrocarbon indicator. A case study: 86th Annual International Meeting, SEG, Expanded Abstracts, 1839-1943, doi.org/10.1190/segam2016-13871199.1.

Partyka, G., Gridley, J. and Lopez, J. [1999] .Interpretational applications of spectral decomposition in reservoir characterization. *The Leading Edge*, **18**(3), 353-360, doi.org/10.1190/1.1438295.

Portniaguine, O. and Castagna, J.P. [2004] Inverse spectral decomposition. 74th Annual International Meeting, SEG, Expanded Abstracts, 1786-1789. doi.org/10.1190/1.1845172.

Portniaguine, O. and Castagna, J.P. [2005] Spectral inversion: Lessons from modeling and Boonesville case study. 75th Annual International Meeting, SEG, Expanded Abstracts, 1638-1641. doi.org/10.1190/1.2148009.

Puryear, C.I., Portniaguine, O., Cobos, C. and Castagna, J.P. [2012]. Constrained least-squares spectral analysis: Applications to seismic data. *Geophysics*, **77**(5), ISO-Z132, doi.org/10.1190/geo2011-0210.1.

Sinha, S., Routh, P.S., Anno, P.D. and Castagna, J.P. [2005]. Spectral decomposition of seismic data with continuous-wavelet transforms. *Geophysics*, **70**(6), 19–25, doi.org/10.1190/1.2127113.

Stockwell, R., Mansinha, L. and Lowe, R. [1996]. Localization of the complex spectrum: the s transform. *IEEE Transactions on Signal Processing*, **44**(4), 998–1001, doi:10.1109/78.492555.

Widess, M.B. [1973]. How thin is a thin bed? *Geophysics*, **38**(6), 1176-1180, doi.org/10.1190/1.1440403.